OPTICA

Color characterization of infrared two-photon vision

Pedro Gil,[1,2,*] Juan Tabernero,[1,2] Silvestre Manzanera,[1,2] Christina Schwarz,[3] and Pablo Artal[1]

[1]Laboratorio de Óptica, Universidad de Murcia, Campus de Espinardo (Edificio 34), Murcia 30100, Spain
[2]Departamento de Electromagnetismo y Electrónica, Facultad de Química, Universidad de Murcia, Murcia 30100, Spain
[3]Institute for Ophthalmic Research, University of Tübingen, Tübingen, Germany
*pedro.gilf@um.es

Received 6 October 2023; revised 14 November 2023; accepted 15 November 2023; published 19 December 2023

Humans have the ability to perceive pulsed near-infrared (NIR) light as visible light with about half the wavelength through a process known as two-photon (2P) absorption. Although it has been known for several decades, color perception in 2P vision remains uncharacterized. In this study, we conducted color matching experiments between pulsed NIR light and continuous visible light. We investigated seven NIR wavelengths ranging from 880 to 1100 nm, along with three radiant power values at the pupil plane, varying from 10 to 30 μW. Through these experiments, we obtained chromatic coordinates, chromaticity diagrams, dominant wavelengths, and average spectra. We found a pronounced correlation between perceived hue and wavelength, with hues shifting from reddish purple at 880 nm to blue, green, and yellowish green at 1100 nm. Moreover, we observed a relationship between hue and power for the wavelengths closer to the visible end of the spectrum. This phenomenon appears to be a consequence of the intensity-dependent ratio between the single photon (1P) and 2P absorption efficiencies of the visual pigments.

https://doi.org/10.1364/OPTICA.507240

1. INTRODUCTION

The human eye is commonly believed to have a range of vision limited to the so-called visible region of the electromagnetic spectrum, with wavelengths ranging from approximately 400 to 700 nm. However, since the early 20th century, it has been known that the human eye retains the ability to detect light in the near-infrared (NIR) region, albeit with reduced retinal sensitivity. Studies showed that foveal sensitivity drops by a factor of 10^6 and 10^{10} for wavelengths of 800 and 1000 nm, respectively, compared to its peak value at 550 nm [1,2].

Subsequently, with the advent of the first lasers, it was observed that when the eye is illuminated with pulsed light it is possible to perceive light in the NIR as visible light with about half the wavelength of the incident light [3–6]. The underlying physical mechanism responsible for this visual phenomenon has been a subject of debate for several decades. Two distinct nonlinear mechanisms have been proposed to try to explain the phenomenon: second harmonic generation (SHG) occurring in the cornea, lens, or retina [4,6–8]; or two-photon (2P) absorption by retinal photopigments [5]. In 2014, Palczewska *et al.* combined biochemical, electrophysiological, and computational tools with psychophysical experiments to provide strong evidence for 2P absorption and a direct photoisomerization of the visual pigments as the most likely cause for this phenomenon [9]. The nonlinear nature of the phenomenon has also been validated by subsequent studies [10].

2P vision provides a variety of avenues for the development of new clinical tests. The ability of the human eye to perceive NIR light under specific conditions, coupled with the higher penetration of IR light in scattering media, is an advantage, for example, for testing retinal response in the cases where ocular opacity does not allow its assessment with conventional techniques. Recently, several studies have been reported exploring this approach by assessing IR light retinal sensitivity and developing the so-called 2P microperimetry [11–16]. Other metrics of visual performance such as visual acuity have also been studied in their 2P counterpart [17].

Despite the efforts to elucidate the nature of the visual phenomenon and its potential applications in a clinical environment, a comprehensive quantitative characterization of color perception in 2P vision has not yet been achieved. Currently, color characterization has only been accomplished to some extent by qualitatively describing the perceived hue or by associating the perceived color with a pure wavelength [3–5,8,9]. To try to fill this gap, in this study we conducted color matching experiments between pulsed NIR and continuous visible light, with the objective of quantitatively characterizing the perceived hue during the 2P vision process while considering different adjustable parameters of the illumination source. Specifically, we investigated the impact of the laser wavelength and the radiant power entering the pupil. We expect that a thorough and quantitative comprehension of color perception in 2P vision will unlock new avenues for research and clinical applications of the phenomenon. In particular, a full understanding of 2P color perception could be the starting point for the development of a 2P retinal display. Such a display could allow us to perceive tunable color images in cases where the opacity

of the ocular media hinders conventional vision, among other potential applications.

2. METHODS

A. Experimental Setup

A combined 1P and 2P retinal projection display, based on a previously developed setup, was used to carry out the psychophysical experiment [10,17]; further details of the system can be found in those references. A schematic diagram of the experimental setup is presented in Fig. 1. A supercontinuum pulsed laser (SuperK COMPACT, NKT Photonics, Birkerød, Denmark) with a broad spectrum spanning from 450 to 2400 nm, pulse durations of the order of 1 ns, and a maximum pulse repetition frequency of 20 kHz was used. Throughout all the color matching experiments, the laser was operated at a fixed pulse repetition frequency of 15 kHz. Regarding stability, the laser exhibits a mean power fluctuation lower than ±1%/h and a pulse–pulse jitter of less than 2 μs.

Throughout all the tests, the exit pupil of the system was set at 1.5 mm. This reduced aperture made the impact of defocus and focus errors caused by the longitudinal chromatic aberration negligible.

Next to the IR stimulus, another stimulus of continuous visible light emitted by an AMOLED microdisplay (SXGA, eMagin Corporation, Hopewell Junction, NY, USA) is projected onto the fovea. The visible stimulus is introduced into the system through lens L5 and a beam splitter (BS). The size and appearance of this stimulus are controlled by custom software; its shape and dimensions are chosen to be the same as those of the IR stimulus.

B. Psychophysical Test

Four healthy volunteers, aged between 22 and 50 years, participated in the study. All participants were either emmetropic or fully corrected, and reported no history of ocular diseases or conditions that could affect the outcome of the study. The presence of color deficiencies was evaluated by means of the 38 plates Ishihara test. All subjects successfully completed the test without errors. They were all members of the lab trained in psychophysical experiments. The study was approved by the Ethics Committee of the University of Murcia (Spain). It followed the tenets of the Declaration of Helsinki, and all subjects gave informed consent prior to any measurement.

The tests were conducted in a dark room in which all possible light sources were minimized ($E_v < 0.1$ lux), including reflections on the system, indicator lights, and monitor light. These conditions served to standardize the experiment for all subjects and allowed us to maximize the contrast between the stimuli (IR and visible) and the background, so that we could work close to the 2P vision thresholds and prevent possible alterations in color perception induced by external light sources. Prior to the start of the experiments, the subjects were dark adapted to these conditions for 20 min. A bite bar was used to maintain the position of the participants during the experiments.

During the tests, the IR and visible stimuli were simultaneously projected side-by-side onto the subjects' fovea. The objective of the participants was to match the perceived color of both stimuli for each combination of wavelength and power at the pupil plane. For this purpose, the subjects could individually modify the hue, saturation, and value (HSV) coordinates of the visible stimulus using a keypad. They were allowed to modify the color coordinates in any order and make as many adjustments as they deemed necessary. Prior to any measurement, the AMOLED display was initialized to the same color in the green zone. The procedure was repeated three times for each of the cases considered. There was a rest time of 2 min between each test. The tests were divided into two sessions. In the first one, the first three wavelengths were measured, while in the second one the remaining four wavelengths were measured.

C. Color Measurement

Following the color matching process between the 2P and the visible stimuli, the chromatic information of the visible light was indirectly obtained using a spectrometer (USB4000, Ocean Optics, Largo, FL, USA). Due to the low light levels involved in the experiments, the measurement of the visible light spectrum was only feasible immediately after the AMOLED display. The

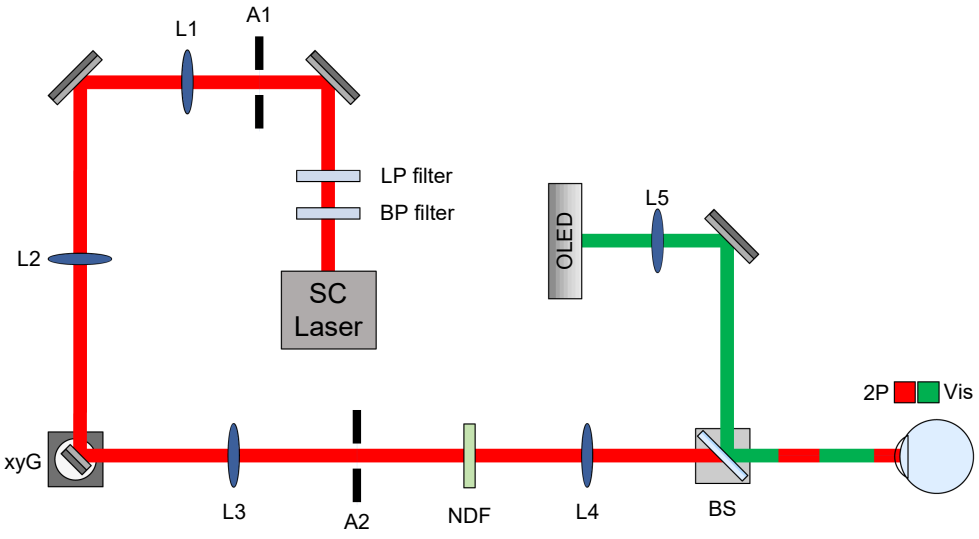

Fig. 1. Schematic representation of the 1P and 2P display. The path of the pulsed IR beam is depicted in red, while the path of the visible beam is represented in green. BP filter, bandpass filter; LP filter, longpass filter; A1 and A2, apertures; L1–5, lenses; xyG, two-axis galvo mirror; NDF, neutral density filter; BS, beam splitter.

visible spectrum was measured between 380 and 780 nm with an integration time of 10 s.

The light from the display passes through a lens (LA1213-A, Thorlabs, Newton, NJ, USA), a mirror (PF10-03-P01, Thorlabs), and a beam splitter (BP233, Thorlabs) before reaching the subject's pupil. To account for any potential color effects introduced by these optical elements, we propagate the spectrum of the light under consideration across all the elements from the transmittance (for the lens) and reflectance (for the mirror and the beam splitter) data provided by the manufacturer.

The resulting spectrum, which corresponds to the light reaching the pupil plane, is then transformed to CIE 1931 chromatic coordinates (x, y) by means of the color matching functions [18,19]. For each case, the average of the three trials performed by the subjects is considered. The associated dominant wavelength is also calculated for each case from the CIE 1931 chromatic coordinates [20,21]. It is defined as the wavelength of a monochromatic light that evokes the same hue perception as the light under consideration when combined with achromatic (white) light. It is obtained from the CIE 1931 diagram by projecting the line connecting the reference white with the color under consideration to the spectral locus. The point at which this line intersects the locus indicates the dominant wavelength [20]. For these calculations, the equienergy point E ($x = 0.33$, $y = 0.33$) is adopted as the achromatic white point.

Despite being a widely used system, the distribution of colors in the CIE 1931 color space is very non-homogeneous in terms of visual perception [22]. Thus, it is convenient to use other systems with a more homogeneous color distribution such as the CIE 1976 Uniform Chromaticity Scale (UCS). The coordinates (u', v') of this diagram can be obtained from the coordinates (x, y) of the CIE 1931 system by means of the following transformations [23]:

$$u' = 4x/(-2x + 12y + 3); \quad v' = 9y/(-2x + 12y + 3).$$

All the calculations for the propagation of the spectrum, its transformation to chromatic coordinates, and averaging have been carried out by means of custom routines programmed in Wolfram Mathematica (Wolfram Research, Champaign, IL, USA).

3. RESULTS

CIE 1931 and CIE 1976 coordinates were obtained for all combinations of NIR wavelength and power at the pupil plane. The between-subject average of the chromatic coordinates is presented in Table 1. Measurements at a power of 10 μW were not feasible for wavelengths above 950 nm because the 2P stimulus lacked brightness for color matching.

To visually analyze the chromatic information, chromaticity diagrams were generated from the chromaticity coordinates (Figs. 2 and 3). For the lower wavelengths (880–920 nm) there is a noticeable hue shift from reddish-purple to blue as both wavelength and power increase. For the higher wavelengths (950–1100 nm), there is a hue shift from blue towards green and yellowish green with increasing wavelength. As can be seen in Fig. 3, there is a greater effect and inter-subject variability in hue perception for lower wavelengths compared to higher wavelengths.

Furthermore, dominant wavelengths were computed from the CIE 1931 coordinates (Table 2). For the cases of 880 nm in all instances and for 900 nm at power values of 10 and 20 μW, it was not possible to define a dominant wavelength, and non-spectral purples were obtained. Therefore, in these cases it is not possible to reproduce the hue under consideration from the mixture of a single monochromatic light and a white (achromatic) light. In those cases where a dominant wavelength could be defined, there is a shift from blue towards yellowish green as the wavelength increases, as is also seen in the chromaticity diagrams. However, no differences in dominant wavelength values were observed across the different power levels considered for each laser wavelength. This suggests that, at wavelengths above 900 nm and for the range of powers considered, the power at the pupil plane does not have a substantial impact on the hue perception.

Table 1. Average CIE 1931 (x, y) and CIE 1976 (u', v') Coordinates of Color-Matched 2P Stimuli[a]

λ_{Laser}, nm	P, μW	x (Δx)	y (Δy)	u' ($\Delta u'$)	v' ($\Delta v'$)
880	10	0.450	0.319	0.303	0.484
		(0.081)	(0.018)	(0.052)	(0.023)
	20	0.414	0.312	0.280	0.474
		(0.089)	(0.019)	(0.058)	(0.025)
	30	0.384	0.310	0.257	0.468
		(0.089)	(0.026)	(0.056)	(0.028)
900	10	0.344	0.302	0.231	0.458
		(0.085)	(0.024)	(0.055)	(0.027)
	20	0.293	0.282	0.202	0.437
		(0.067)	(0.019)	(0.043)	(0.022)
	30	0.247	0.269	0.172	0.422
		(0.047)	(0.015)	(0.030)	(0.017)
920	10	0.254	0.277	0.174	0.428
		(0.026)	(0.012)	(0.015)	(0.011)
	20	0.206	0.256	0.145	0.407
		(0.042)	(0.014)	(0.027)	(0.016)
	30	0.189	0.2517	0.134	0.401
		(0.030)	(0.0094)	(0.020)	(0.011)
950	20	0.186	0.278	0.1245	0.418
		(0.013)	(0.031)	(0.0043)	(0.022)
	30	0.1619	0.261	0.1115	0.404
		(0.0065)	(0.016)	(0.0039)	(0.011)
1000	20	0.245	0.438	0.127	0.506
		(0.015)	(0.043)	(0.011)	(0.018)
	30	0.237	0.451	0.1197	0.510
		(0.015)	(0.048)	(0.0066)	(0.020)
1050	20	0.273	0.466	0.136	0.5210
		(0.018)	(0.023)	(0.013)	(0.0070)
	30	0.275	0.504	0.1298	0.5336
		(0.012)	(0.020)	(0.0078)	(0.0060)
1100	20	0.3234	0.490	0.1572	0.5354
		(0.0067)	(0.014)	(0.0008)	(0.0052)
	30	0.3266	0.5038	0.1557	0.5402
		(0.0064)	(0.0085)	(0.0040)	(0.0026)

[a] λ_{Laser} and P are the considered laser wavelength and power at the pupil plane, respectively. Δx, Δy, $\Delta u'$, and $\Delta v'$ represent standard deviations.

In Fig. 4 the dominant wavelength is plotted against the laser wavelength for a fixed power level of 30 μW, as it contains the largest number of available data points. It is observed that the points corresponding to lower wavelengths (900–950 nm) deviate considerably from the ideal line $\lambda_D = \lambda_{Laser}/2$, shifting towards longer wavelengths. Conversely, as the laser wavelength increases, the points tend to approach the ideal line (Fig. 4).

Lastly, the average matched spectrum of the visible light stimulus was computed for all subjects at each wavelength and power combination (Fig. 5). It can be seen that for the 880 and 900 nm wavelengths there is a notable contribution from both a peak in the

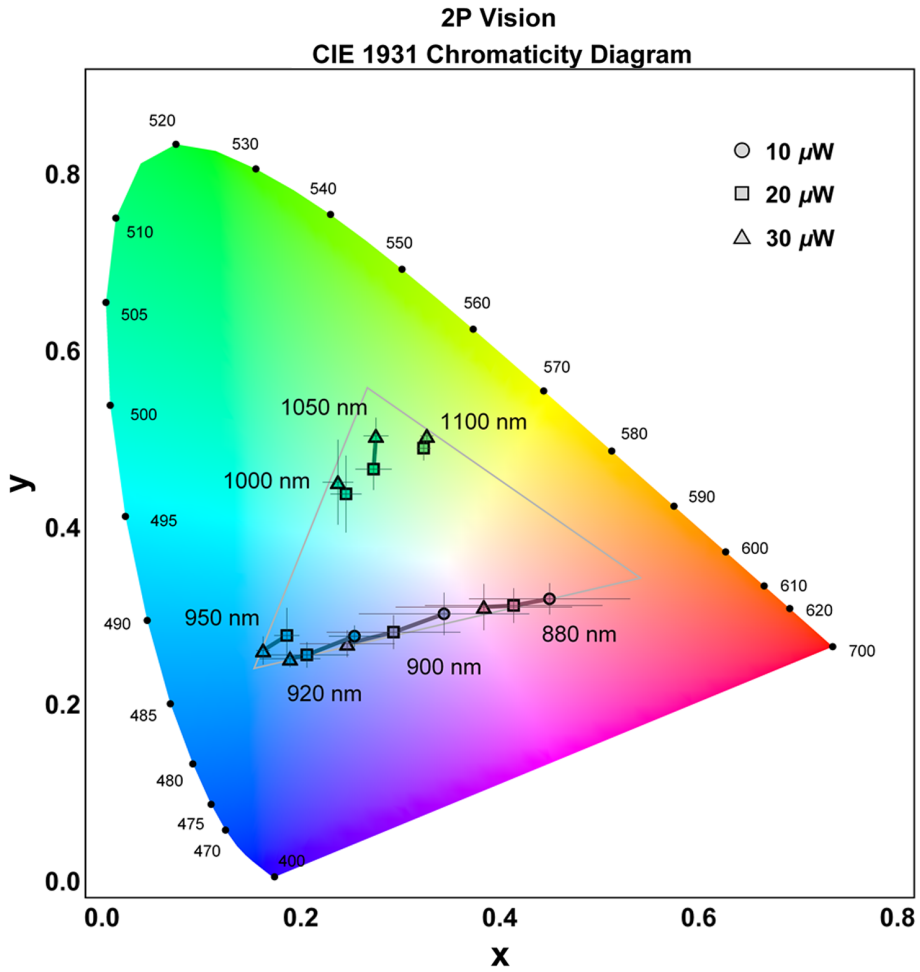

Fig. 2. CIE 1931 chromaticity diagram displaying average coordinates of color matched 2P stimuli. Points corresponding to the same wavelength are connected by lines. Each considered power is represented by a different symbol: circle for 10 μW, square for 20 μW, and triangle for 30 μW. The error bars represent a standard deviation in the x and y coordinates. The gray triangle represents the gamut of the display propagated to the pupil plane.

blue region and a peak in the red region. It can also be seen that for 880–920 nm, for a normalized contribution of the blue peak, there is a decrease in the contribution of the red peak with increasing power.

4. DISCUSSION

A psychophysical experiment has been conducted to study and quantitatively characterize the perceived hue during the 2P vision process as a function of the NIR wavelength and the radiant power passing through the pupil. It should be noted that the NIR wavelengths were selected using filters that provide beams that are not monochromatic. This could have some effect on the perceived hue. Moreover, the filtering of the supercontinuum laser might alter the pulse duration, and this may have some impact on the color comparison between wavelengths, especially for the lower ones. In addition, higher order aberrations have not been corrected during the experiments, but their impact should be largely reduced by limiting the beam diameter entering the eye.

A strong dependence of the perceived hue with wavelength has been observed, shifting from reddish purple at 880 nm to blue, green, and finally to yellowish green at 1100 nm. These findings are consistent with previous studies [3,5,7,9]. The gamut of the AMOLED display is the main limitation of the experiment. As can be seen in Figs. 2 and 3, most of the points fall close to the boundaries that enclose the gamut. This suggests that the subjects would have chosen more saturated colors, if possible, during the color matching process. Therefore, using a display with a wider gamut would provide more accurate measurements.

A dependence of the perceived hue on power at the pupil plane has also been found for the lower wavelengths, but not for the higher ones. This phenomenon, observed mainly at wavelengths approaching the end of the visible spectrum, is presumably due to the combined effect of conventional one-photon (1P) vision, resulting from the linear absorption of light from the IR tails, and the nonlinear 2P vision process. Indeed, the likelihood of 2P absorption increases quadratically with the average power of the incident light beam, whereas the likelihood of 1P absorption increases linearly with beam power [24]. These different dependencies would cause a change in the spectrum of the perceived light, which would translate into the observed hue shift.

The distribution of the spectral peaks (Fig. 5) allowed us to gain a deeper insight into how hue perception varies with power. The existence of a relevant contribution from both a red peak and a blue peak in the 880 and 900 nm spectra is consistent with the impossibility of defining a single dominant wavelength (Table 2) and with the upward deviation of the dominant wavelength from half the laser wavelength in these cases (Fig. 4). Moreover, it has

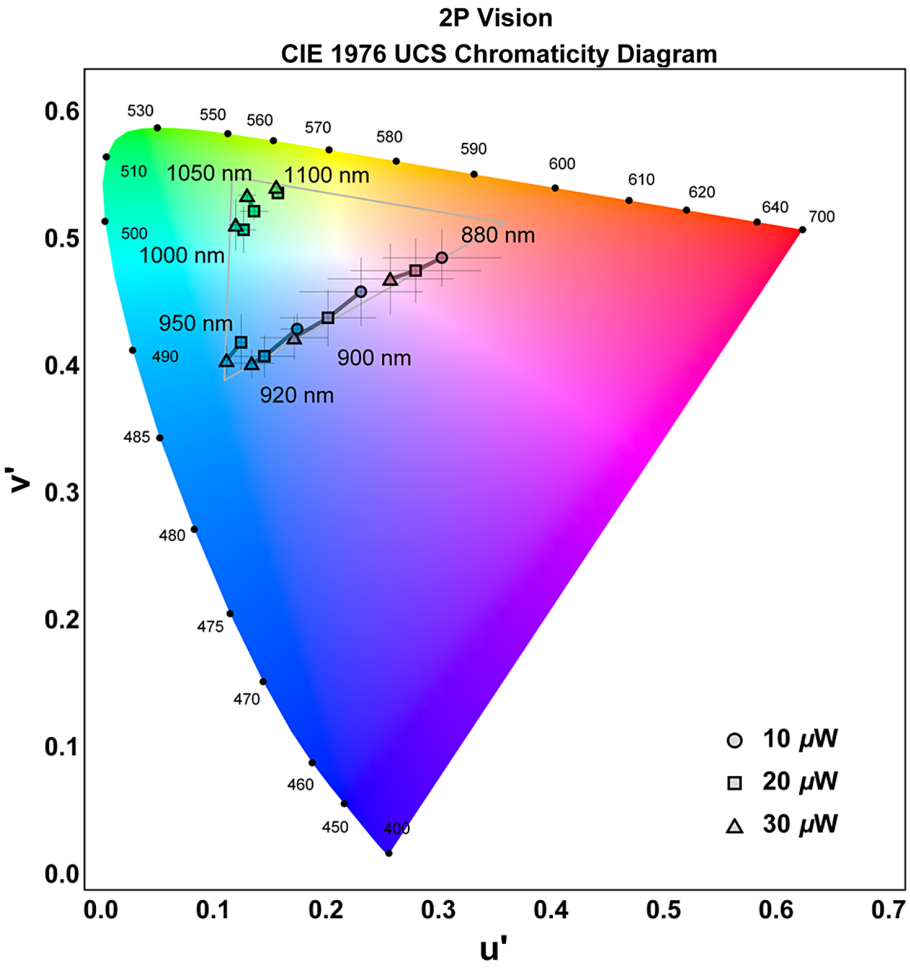

Fig. 3. CIE 1976 UCS chromaticity diagram of the average coordinates. Points corresponding to the same wavelength are connected by lines. Each considered power is represented by a different symbol: circle for 10 μW, square for 20 μW, and triangle for 30 μW. The error bars represent a standard deviation in the u' and v' coordinates. The gray triangle represents the gamut of the display propagated to the pupil plane.

Table 2. Average Dominant Wavelength (λ_D) as a Function of Laser Wavelength and Power at the Pupil Plane[a]

	$\lambda_D(\Delta\lambda_D)$, nm		
λ_{Laser}, nm	10 μW	20 μW	30 μW
880	-	-	-
900	-	-	478 (10)
920	482 (2)	483 (2)	484 (1)
950		487 (3)	486 (2)
1000		510 (12)	510 (9)
1050		525 (11)	533 (7)
1100		551 (4)	553 (2)

[a]$\Delta\lambda_D$ represents the mid-range of the dominant wavelength values. Each cell is colored with the approximate color of the corresponding dominant wavelength.

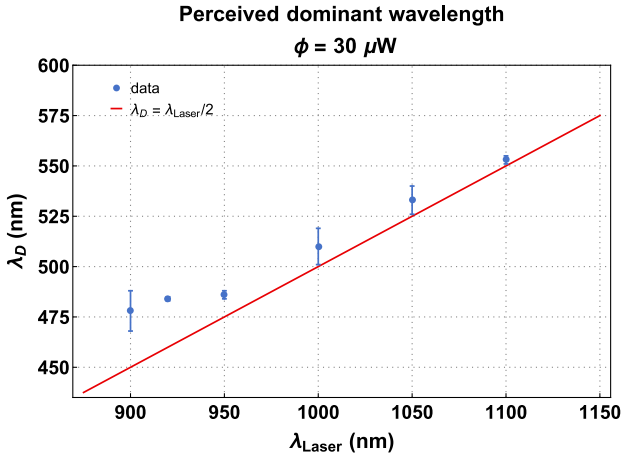

Fig. 4. Dominant wavelength against laser wavelength for a fixed power of 30 μW at the pupil plane. The red line represents half the wavelength of the laser beam, corresponding to the expected ideal case in 2P vision. The experimental data points and their mid-range are depicted in blue.

been observed that for 880–920 nm the contribution of the blue peak increases while the contribution of the red peak decreases with increasing power. This trend is not observed for the other wavelengths. From 950 nm onwards, the relative magnitude of the spectral peaks remains constant with power, which would imply a dominance of the 2P absorption phenomenon for all powers. Therefore, the 1P vision mechanism would contribute to the

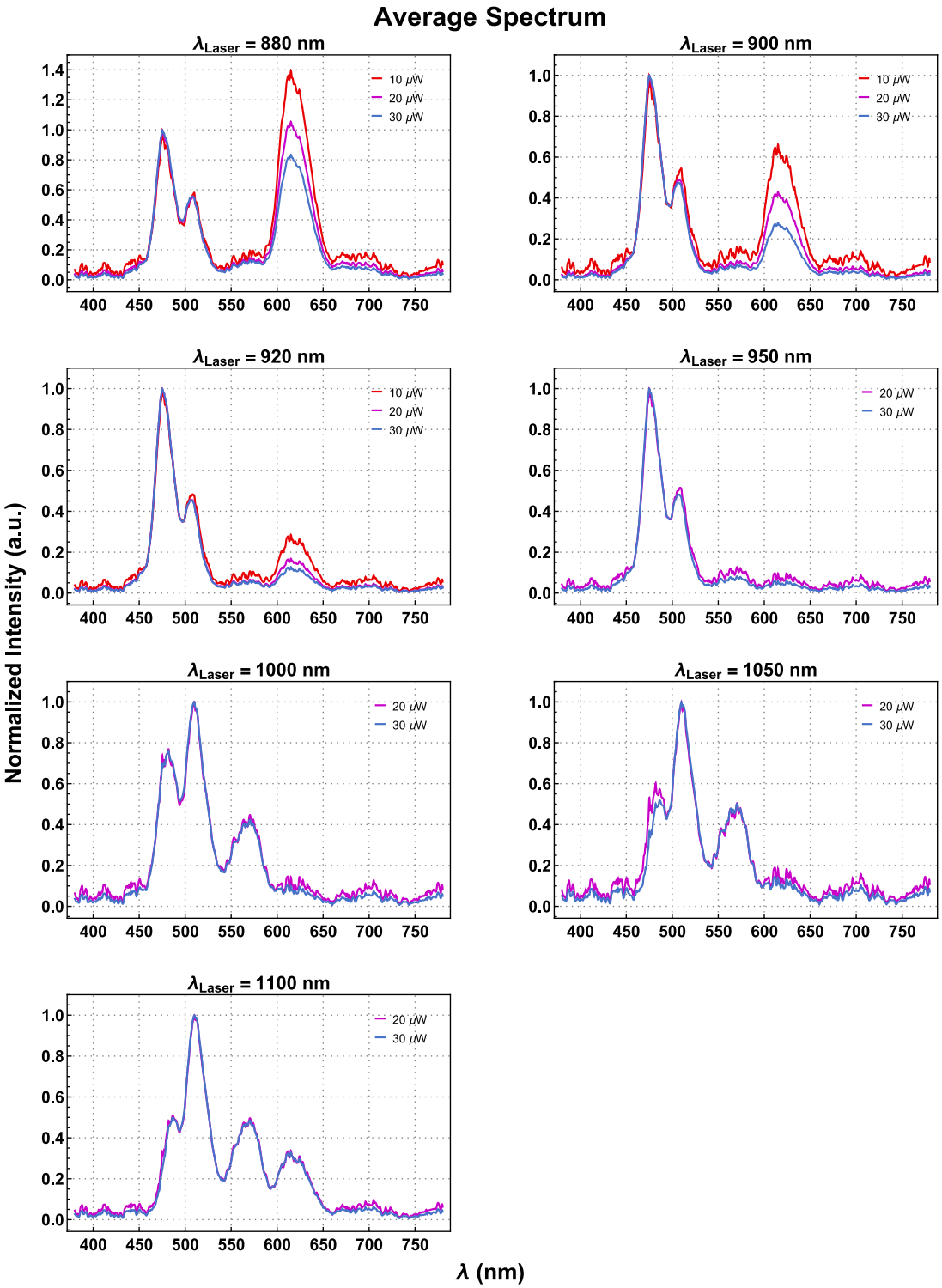

Fig. 5. Average spectrum of the matched visible stimulus (between 380 and 780 nm) as a function of NIR wavelength and power at the pupil plane. Spectra corresponding to $\lambda_{Laser} = 880$ nm are normalized to the first peak for ease of comparison. The remaining spectra are normalized to the largest peak. The spectra corresponding to 10 μW of power are shown in red, those for 20 μW are shown in purple, and those for 30 μW are shown in blue.

perceived color with a red component that decreases its relative weight as both power and wavelength increase. The coexistence of 1P and 2P vision could potentially be applied in the diagnosis of retinal dysfunction. Photoreceptor damage could alter the ratio between 1P and 2P absorption, which would result in a divergence of the perceived hue compared to a healthy eye.

It should be noted that in this experiment we kept the laser repetition rate and pulse width, as well as the numerical aperture of the system, constant. It would be expected that these results would vary for other operating conditions. Future work in this direction would include a study of the influence of the remaining adjustable laser parameters on the perceived color. A full understanding of

this influence would allow the relative presence of both types of vision (1P and 2P) to be regulated at will. This could be used in 2P retinal displays where RGB stimuli are presented by using only infrared light. Since the color percepts result from the same NIR wavelength, the red and blue components of such a stimulus would be focused on the same plane. Moreover, a green component corresponding to 1050 nm would present a modest defocus of about 0.2 D with respect to the 880 nm wavelength [25]. Therefore, an RGB stimulus based on 2P vision would be nearly free of longitudinal chromatic aberration (CA). Transverse CA is also expected to be minor. A 2P retinal display with minimal CA may be of great interest in the field of virtual reality (VR), where optimal visual fidelity is required. Notably, some commonly used commercial devices exhibit a noticeable amount of transverse CA [26]. By adopting a 2P retinal display these chromatic issues could be effectively addressed, potentially improving the VR experience.

Regarding the distribution of the data, we noticed that for the lower wavelengths there is a greater dispersion between subjects (Table 1, Fig. 3). This could be due to small misalignments during the measurement process. Despite the use of a bite bar to fixate the subjects' position throughout the experiment, small head movements may occur. These subtle movements could result in decentrations where the beam enters the pupil off-axis while the focal point remains at (or near) the fovea. In these cases, the Stiles–Crawford effect may occur. Alternatively, rotations may take place in which the beam enters the center of the pupil, but the image is projected outside the fovea, so that waveguiding is efficient but the distribution of photoreceptors changes. These effects independently or combined could modify the perceived color. We have qualitatively tested this situation and found that the hue variations are more pronounced at lower wavelengths, which is consistent with the results obtained. For higher wavelengths, misalignments result in a decreased brightness of the stimulus rather than a hue shift. This opens new avenues to investigate the variation of color perception when the infrared stimulus is presented at retinal locations other than the center of the fovea, as well as how the Stiles–Crawford effect is manifested in 2P vision.

5. CONCLUSIONS

We conducted a psychophysical experiment to quantitatively characterize the effect of different adjustable parameters in the illumination source, specifically the wavelength and the radiant power entering the pupil, on the perception of hue during the 2P vision process.

We found a strong dependence of perceived hue on wavelength in the NIR, which is in good agreement with previous works [3,5,7,9]. We also found that the perceived hue exhibits a dependence on radiant power, especially for NIR wavelengths closer to the end of the visible spectrum. This visual effect appears to be the result of the linear versus squared dependence on intensity of 1P and 2P absorption. To date, this phenomenon has not been considered in safety standards, visual stimulation paradigms, or color theory and offers additional degrees of freedom for the generation of metamers.

APPENDIX A: LASER SAFETY CALCULATIONS

A detailed description of the safety calculations is presented in this appendix. The calculations are based on the ANSI Z136.1-2014 standard and the paper by Delori *et al.* in which they formulate the limits imposed by the ANSI standards with emphasis on ophthalmic devices [27,28].

We worked with a pulsed supercontinuum laser with pulse duration $t_1 = 1$ ns, a repetition rate of $F = 15$ kHz, and seven narrow bands with center wavelengths $\lambda_{\text{Laser}} = \{880, 900, 920, 950, 1000, 1050, 1100\}$ nm. Our stimulus consisted of a square subtending an angle of 4×4 arcmin (or 1.2 mrad). This is below the minimum angle for which the standard considers it an extended source, $\alpha_{\min} = 1.5$ mrad [27,28]. Therefore, the calculations are performed considering the stimulus as a point source. Although each trial lasted approximately 60 s and subjects had a 2 min pause before performing the next trial, we adopted the conservative approach of considering the sum of all trials as the exposure time T. As it was more restrictive, we considered the total number of measurements of the first session for the calculation of the limits. Thus, $T = (3\ \text{wvls}) \times (3\ \text{powers}) \times (3\ \text{trials}) \times (60\ \text{s}) = 1620$ s. Since we did not limit the time that subjects spent on each trial, we further restricted the limits by extending the exposure time to $T = 2000$ s.

For repetitive-pulse lasers, the most restrictive maximum permissible exposure (MPE) at the cornea obtained from three rules must be chosen [27,28]:

1. *single-pulse limit*:

$$\text{MPE}\,(t_1) \quad \text{in J/cm}^2,$$

2. *average-power limit*:

$$\text{MPE}\,(T)\,/n \quad \text{in J/cm}^2,$$

3. *repetitive-pulse limit*:

$$C_P \text{MPE}\,(t_1) \quad \text{in J/cm}^2,$$

where $n = F\,T$ is the number of pulses, and $C_P = 1$ for this combination of source size and pulse duration. Since the duration of the pulses t_1 is smaller than $t_{\min}$ (5 μs for $400 < \lambda < 1050$ nm, and 13 μs for $1050 < \lambda < 1400$ nm) in all cases, rule 3 must be evaluated using $t_1 = t_{\min}$. The evaluation of the three rules shows that rule 2 is the most restrictive in all cases. We use a power meter to measure the radiant power in the plane of the pupil, so it is convenient to express the safety limits in terms of radiant power through the pupil MPΦ [28]:

$$\text{MP}\Phi\,(T) = \text{MPE}\,(T)\,\frac{A_{p,7}}{P} \quad \text{in W},$$

where $A_{p,7}$ is the area of a 7 mm pupil ($A_{p,7} = 0.385$ cm^2), as suggested by the standard [27,28]; and P is a pupil factor ($P = 1$ for all considered wavelengths). The MPEs are given by [27]

$$\text{MPE}\,(T) = C_A \times 10^{-3}\ \text{W/cm}^2 \quad \text{for } 700 < \lambda < 1050\ \text{nm},$$

$$\text{MPE}\,(T) = 5C_C \times 10^{-3}\ \text{W/cm}^2 \quad \text{for } 1050 < \lambda < 1200\ \text{nm},$$

with $C_A = 10^{0.002(\lambda - 700)}$ and $C_C = 1$. Table 3 shows the resulting safety limits for each wavelength considered during the experiments. As can be seen, the maximum power used of 30 μW is a factor of 29 to 64 below the safety limits in all cases.

Exposures to several wavelengths are additive on a proportional basis. To comply with the safety standard, the summed ratios must be smaller than one. Taking this into account, we operated a factor of three below the safety limit.

Table 3. MPΦ Entering the Pupil for Each Wavelength in the NIR

λ, nm	880	900	920	950	1000	1050	1100
MPΦ, μW	882	967	1060	1218	1533	1930	1925

Funding. Fundación Séneca (21602/FPI/21); European Research Council (852220); Ministerio de Ciencia, Innovación y Universidades (PID2019-105639RA-I00, PID2019-105684RB-I00/AEI/10.13039/501100011033).

Disclosures. The authors declare no conflicts of interest.

Data availability. Data underlying the results presented in this paper are not publicly available at this time but may be obtained from the authors upon reasonable request.

REFERENCES

1. C. F. Goodeve, "Relative luminosity in the extreme red," Proc. R. Soc. London A **155**, 664–683 (1936).
2. D. R. Griffin, R. Hubbard, and G. Wald, "The sensitivity of the human eye to infra-red radiation," J. Opt. Soc. Am. **37**, 546–554 (1947).
3. L. S. Vasilenko, V. P. Chebotaev, and Y. V. Troitskii, "Visual observation of infrared laser emission," Sov. Phys. JETP **21**, 513–514 (1965).
4. D. H. Sliney, R. T. Wangemann, J. K. Franks, *et al.*, "Visual sensitivity of the eye to infrared laser radiation," J. Opt. Soc. Am. **66**, 339–341 (1976).
5. V. G. Dmitriev, V. N. Emel'yanov, M. A. Kashintsev, *et al.*, "Nonlinear perception of infrared radiation in the 800–1355 nm range with human eye," Sov. J. Quantum Electron. **9**, 475 (1979).
6. T. Theodossiou, E. Georgiou, V. Hovhannisyan, *et al.*, "Visual observation of infrared laser speckle patterns at half their fundamental wavelength," Lasers Med. Sci. **16**, 34–39 (2001).
7. Q. Zaidi and J. Pokorny, "Appearance of pulsed infrared light: second harmonic generation in the eye," Appl. Opt. **27**, 1064–1068 (1988).
8. P. V. Kazakevich, A. V. Simakin, and G. A. Shafeev, "Frequency up-conversion of infrared laser radiation in the human retina," Laser Phys. **16**, 1078–1081 (2006).
9. G. Palczewska, F. Vinberg, P. Stremplewski, *et al.*, "Human infrared vision is triggered by two-photon chromophore isomerization," Proc. Natl. Acad. Sci. USA **111**, E5445–E5454 (2014).
10. S. Manzanera, D. Sola, N. Khalifa, *et al.*, "Vision with pulsed infrared light is mediated by nonlinear optical processes," Biomed. Opt. Express **11**, 5603–5617 (2020).
11. D. Ruminski, G. Palczewska, M. Nowakowski, *et al.*, "Two-photon microperimetry: sensitivity of human photoreceptors to infrared light," Biomed. Opt. Express **10**, 4551–4567 (2019).
12. A. Wei, U. V. Mehta, G. Palczewska, *et al.*, "Two-photon microperimetry: a media opacity-independent retinal function assay," Transl. Vis. Sci. Technol. **10**, 11 (2021).
13. M. J. Marzejon, Ł. Kornaszewski, J. Bogusławski, *et al.*, "Two-photon microperimetry with picosecond pulses," Biomed. Opt. Express **12**, 462–479 (2021).
14. G. Labuz, A. Rayamajhi, R. Khoramnia, *et al.*, "The loss of infrared light sensitivity of photoreceptor cells measured with two-photon excitation as an indicator of diabetic retinopathy: a pilot study," RETINA **41**, 1302–1308 (2021).
15. G. Łabuz, A. Rayamajhi, K. Komar, *et al.*, "Infrared- and white-light retinal sensitivity in glaucomatous neuropathy," Sci. Rep. **12**, 1961 (2022).
16. G. Łabuz, A. Zielińska, L. J. Kessler, *et al.*, "Two-photon vision in age-related macular degeneration: a translational study," Diagnostics **12**, 760 (2022).
17. P. Artal, S. Manzanera, K. Komar, *et al.*, "Visual acuity in two-photon infrared vision," Optica **4**, 1488–1491 (2017).
18. *Recommandations officielles de la Commission Internationale de l'Éclairage, Huitième Session, 1931* (Cambridge University, 1932), pp. 19–29.
19. Institute of Ophthalmology (University College London), "CIE 1931 2-deg, XYZ CMFs, CVRL Database," http://www.cvrl.org/.
20. R. W. G. Hunt and M. R. Pointer, *Measuring Colour* (John Wiley & Sons, 2011).
21. "CIE 1931 Demo," https://luminus-cie1931-demo.anvil.app.
22. W. D. Wright, "The sensitivity of the eye to small colour differences," Proc. Phys. Soc. **53**, 93 (1941).
23. J. Schanda, *Colorimetry: Understanding the CIE System* (Wiley, 2007).
24. R. W. Boyd, *Nonlinear Optics* (Academic, 2020).
25. E. J. Fernández and P. Artal, "Ocular aberrations up to the infrared range: from 632.8 to 1070 nm," Opt. Express **16**, 21199–21208 (2008).
26. R. Beams, A. S. Kim, and A. Badano, "Transverse chromatic aberration in virtual reality head-mounted displays," Opt. Express **27**, 24877–24884 (2019).
27. "American National Standard for Safe Use of Lasers," ANSI Z136.1-2014.
28. F. C. Delori, R. H. Webb, D. H. Sliney, *et al.*, "Maximum permissible exposures for ocular safety (ANSI 2000), with emphasis on ophthalmic devices," J. Opt. Soc. Am. A **24**, 1250–1265 (2007).